J Mater Sci: Mater Electron (2017) 28:7928–7934
DOI 10.1007/s10854-017-6494-5

Piezoelectric grain-size effects of $BaTiO_3$ ceramics under different sintering atmospheres

Bowen Dai[1] · Xiaoping Hu[1] · Renqiang Yin[1] · Wangfeng Bai[2] · Fei Wen[1] · Jiangxia Deng[1] · Liang Zheng[1] · Juan Du[3] · Peng Zheng[1] · Huibin Qin[1]

Received: 12 October 2016 / Accepted: 30 January 2017 / Published online: 11 February 2017

Abstract Two groups of barium titanate ($BaTiO_3$) ceramics with high piezoelectric coefficient (d_{33}) have been successfully fabricated by the conventional solid-state reaction technique under different sintering atmospheres. The influences of sintering atmosphere on piezoelectric grain-size effects were systematically investigated. It was found that d_{33} first increases then decreases with the increase of grain size (g) for both two groups of ceramics. However, the d_{33} value reaches the maxima (501pC/N) at $g = 1.13$ μm for the samples sintered under the air sintering atmosphere ($BaTiO_3$–Air). The samples sintered under the oxygen atmosphere ($BaTiO_3$–O_2) exhibit a large d_{33} (>450pC/N) plateau at g from 0.98 to 7.30 μm. The experimental results indicated that the piezoelectric grain-size effects of $BaTiO_3$ ceramics were strongly affected by the sintering atmosphere. Related mechanisms may be attributed to the variations of the domain configuration under different sintering atmospheres.

1 Introduction

$BaTiO_3$ ceramics are historically the first polycrystalline piezoelectric materials and extensively used as piezoelectric actuators, sensors, and transducers [1–4]. During past several decades, $BaTiO_3$ ceramics have been believed to exhibit modest piezoelectric activity, with d_{33} values of approximately 191pC/N, which were inferior to lead zirconate-titanate [5–7]. However, recent studies revealed that amazing high-performance $BaTiO_3$ ceramics can be obtained by means of optimizing raw materials, stoichiometry and processing technique. High d_{33} values (486pC/N, 519pC/N and 788pC/N, respectively) have recently been obtained in $BaTiO_3$ ceramics prepared by solid-state reaction with ordinary $BaCO_3$ and TiO_2 raw powers, two-step sintering using hydrothermally synthesized $BaTiO_3$ fine power and template grain growth technique, respectively [9–12]. These steps forward bring great hope that $BaTiO_3$-based ceramics might be revitalized as a popular lead-free piezoelectric material with the important advantage of being low in cost.

A systematic examination of the literature reveals the existence of a puzzling issue, wherein the reported behaviors of the $BaTiO_3$ ceramics are not unique but display a heterogeneous relationship between the piezoelectric properties and the microstructure [13–15]. Similarly to the well-known dielectric grain-size effects, piezoelectric grain-size effects have been studied by several investigators in the past few years, which the $BaTiO_3$ ceramics display an increase in d_{33} with a decreasing average g, passing through a maximum when $g \sim 1.0$ μm and then decreasing with a further reduction of g [16–22]. Nevertheless, in recent study, other $BaTiO_3$ ceramics display entirely different piezoelectric behaviors, where the change of d_{33} as a function of g does not obey the rule suggested by the piezoelectric grain-size effects [23]. Instead, relatively high d_{33} value are observed in coarse-grained $BaTiO_3$ ceramics with g values large than 10 μm and up to several tens of micrometers [9, 12, 23–25]. These differences demonstrate that previous cognitive on piezoelectric grain-size effects of $BaTiO_3$ ceramics

✉ Peng Zheng
zhengpeng@hdu.edu.cn

[1] College of Electronics and Information, Hangzhou Dianzi University, Hangzhou 310018, China

[2] College of Materials and Environmental Engineering, Hangzhou Dianzi University, Hangzhou 310018, China

[3] School of Materials Sciences and Engineering, Liaocheng University, Liaocheng 252059, China

is insufficient [9, 20–24]. Further systematic investigations are necessary to clarify the underlying mechanism.

On the other hand, it is widely accepted that the preparation condition is one of the most important factors that affects the piezoelectric properties of $BaTiO_3$ ceramics, as it will introduce different defect levels into the ceramics, which could greatly affect the domain configurations and weaken the domain wall movement [12–18, 23]. Considering the point defects tend to migrate to the grain boundaries, the pining effects may be sensitive to fabrication process [9, 24–28]. This may be an important reason for the different piezoelectric grain-size effects reported by different investigators [12, 26–32]. In previous reports, the effects of different preparing processes on the piezoelectric grain-size effects have been systematically studied [9, 16, 22–26]. However, as an important method to control defect levels of the ceramics, systematic investigations on the sintering atmospheres dependence of domain configurations and piezoelectric properties in $BaTiO_3$ ceramics are still rare. Therefore, in this work, we attempted to introduce different defect levels into $BaTiO_3$ ceramics by fabricating two groups of ceramics under air and oxygen sintering atmosphere by the conventional solid-state reaction. The relationships between piezoelectric properties and microstructures for the two groups of ceramics were systematically examined. Possible mechanisms that lead to the different piezoelectric grain-size effects were investigated.

2 Experimental procedure

$BaTiO_3$ powders were prepared by the conventional solid-state reaction technique, starting from properly choosing the raw materials of commercial $BaCO_3$ powder (purity ≥99.0%, Sinopharm Chemical Reagent Co. Ltd.) and TiO_2 powder (purity ≥99.8%, Xiantao Zhongxing Electronic Material Co. Ltd.). The preparation procedures are basically the same as those in previous studies [7, 13, 18, 23]. The raw materials were weighed according to the stoichiometric ratio and ball-milled in ethanol for 12 h on a planetary ball mill. The milled slurry mixture was dried and ground using an agate mortar and pestle. The powder mixture was calcined at 1050 °C for 4 h, followed by a second ball-milling in ethanol procedure for 12 h. This powder was mixed with a 0.5 wt% polyvinyl alcohol (PVA) binder, and pressed into small disks (15 mm in diameter and 1.5 mm in thickness) at 200 MPa. The PVA binder was then burned out at 650 °C for 0.5 h [13, 23]. Finally, $BaTiO_3$ ceramics were sintered at different temperatures (from 1190 to 1450 °C) and under different sintering atmospheres (air environment and oxygen environment, with oxygen rate is 6 ml/min) for 2 h.

The density of the ceramics was measured by the Archimedes method. For piezoelectric properties characterization, the ceramic specimens were coated with silver paint on the top and bottom surfaces and fired at 575 °C for 20 min. Poling was carried out at 80 °C in silicon oil under 5.0 kV/mm for 30 min. Measurements of the piezoelectric properties were taken out after 24 h. The d_{33} value was measured using a Berlicourt-type d_{33} meter (YE 2730 A). The microstructure and domain configuration of the $BaTiO_3$ ceramics were examined using a scanning electron microscope (SEM, JEOL JSM6460), based on which the average grain size (g) and domain width (w) were calculated. g and w were measured as follows: First, four straight lines connecting two diagonal lines; and two straight lines across midpoint were drawn in the micrograph. Second, the total length of the four straight lines was measured using the scale and the total grain number was calculated. Finally, the total length was divided by the total grain number to obtain the average g. Several graphs were plotted to improve the accuracy. For the microstructure and domain configuration characterization, the poled specimens were mirror-polished and chemically etched for 10 s in an aqueous solution of 5%HCl with a small amount of HF (3 drops of HF: 20 ml HCl solution).

3 Results and discussion

The relative density (ρ_0) of the two groups of $BaTiO_3$ ceramics sintered under different sintering atmospheres and different temperature conditions are listed in Table 1. Relative density was calculated using the theoretical density of 6.017 g/cm^3 for the pure $BaTiO_3$ ceramics [15–17]. As shown, for the $BaTiO_3$ ceramics sintered at temperatures above 1230 °C, the ρ_0 of both groups of specimens could reach nearly 98%. Further enhancing the

Table 1 Room temperature physical properties of $BaTiO_3$ ceramics sintered different sintering atmospheres and different temperature conditions

Sintering temperature (°C)	$BaTiO_3$–Air		$BaTiO_3$–O_2	
	ρ_0 (%)	d_{33} (pC/N)	ρ_0 (%)	d_{33} (pC/N)
1190	95.4	275	95.1	244
1210	97.9	501	96.0	465
1230	98.0	485	97.9	495
1250	97.9	465	97.9	499
1270	97.6	346	98.0	410
1300	97.5	318	97.7	356
1350	97.6	307	97.8	344
1400	97.7	292	97.8	313
1450	97.8	303	97.7	309

sintering temperature cannot improve the ρ_0 value. However, the densification temperatures are different for each group specimens. The relative density of $BaTiO_3$–Air specimens is higher than 96% when sintering temperature is above 1190 °C. While for $BaTiO_3$–O_2 specimens, the sintering temperatures have to be increased to 1230 °C to get specimens with relative density higher than 96%.

The dependence of the d_{33} value on the sintering temperature is also shown in Table 1. It could be found that for both groups of specimens, the d_{33} values firstly increase then decreases with the increase of sintering temperature. The d_{33} values increased significantly above 1190 °C for $BaTiO_3$–Air and $BaTiO_3$–O_2 atmosphere. The increase of relative density may be one important reason. High d_{33} value (≈500pC/N) can be obtained in both groups of $BaTiO_3$ ceramics. However, there are some differences in detail. For the $BaTiO_3$–Air specimens, the d_{33} value reaches maximum values of 501pC/N at 1210 °C. While for the $BaTiO_3$–O_2 specimens, the highest d_{33} value of 499pC/N is obtained at the sintering temperature of 1250 °C. In addition, below 1230 °C the $BaTiO_3$–Air ceramics exhibit larger d_{33} values than $BaTiO_3$–O_2 ceramics at the same sintered temperature. While above 1230 °C, $BaTiO_3$–O_2 ceramics exhibit larger d_{33} values.

The piezoelectric properties are considered to be closely related to the microstructure of the $BaTiO_3$ ceramics in the previous study [4, 7, 18–20]. Figure 1 shows SEM images of two groups of various $BaTiO_3$ ceramics sintered under different temperature and different sintering atmosphere conditions. As shown, both groups of ceramics exhibit similar microstructure with uniform g distribution, although the ceramics sintered under different sintering atmospheres. The relationship between sintering temperature and g under different sintering environment is shown in Fig. 2. It can be seen that for all the two groups of $BaTiO_3$ ceramics, the g increases with the increase of sintering temperature. The g can be reach over 30 μm at the highest sintering temperature of 1450 °C. At the same sintering temperature, both groups of $BaTiO_3$ ceramics exhibited similar g, which demonstrates that the sintering atmospheres have less influence on grain growth of $BaTiO_3$ ceramics.

Figure 3 presents the change in d_{33} with g measured at room temperature in all the poled $BaTiO_3$ ceramics. It is clear that d_{33} value was strongly affected by g. As can be seen, both of the groups of the ceramics exhibit

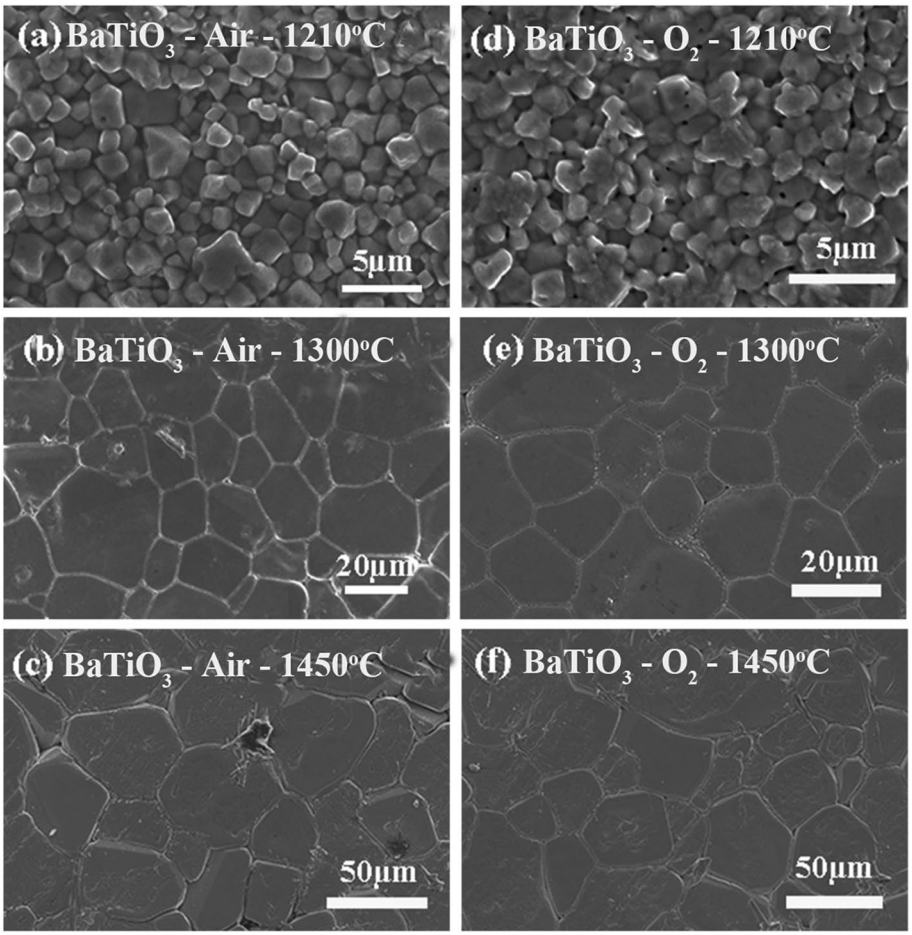

Fig. 1 SEM images of $BaTiO_3$ ceramics sintered under different temperature and different sintering atmosphere conditions

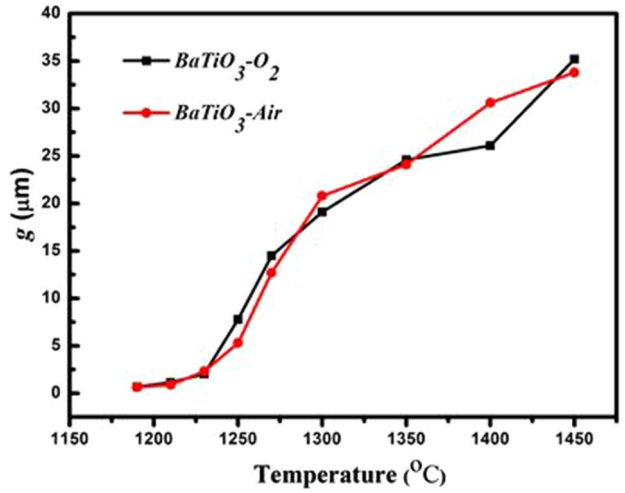

Fig. 2 Temperature dependences of grain size of $BaTiO_3$ ceramics under different sintering atmospheres

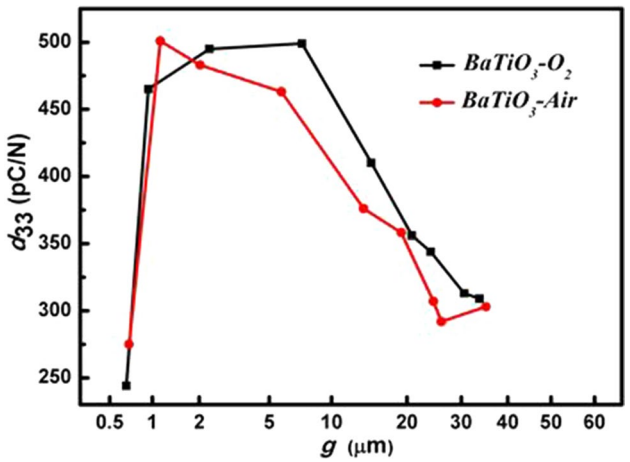

Fig. 3 Grain size dependences of d_{33} of $BaTiO_3$ ceramics under different sintering atmospheres

similar trends of d_{33} with g, the d_{33} value first increases then decreases with the increase of g. The result is generally consistent with the results obtained in previous investigations [6, 8–12]. However, differences could also be observed between the ceramics sintered under the different sintering atmospheres. Firstly, for the $BaTiO_3$–Air ceramics, the largest d_{33} value of 501pC/N obtained at $g = 1.13$ μm. While for the $BaTiO_3$–O_2 ceramics, the maximum piezoelectric constant has been migrated in the direction of large grain. The maximum d_{33} value of 499pC/N is obtained at $g = 7.30$ μm. Secondly, the g dependence of d_{33} exhibits a sharp peak for the $BaTiO_3$–Air ceramics. While for the $BaTiO_3$–O_2 ceramics, the ceramics exhibit a large d_{33} (>450pC/N) plateau at g from 0.98 to 7.30 μm. Furthermore,it should be noted that when $g > 2$ μm, the $BaTiO_3$–O_2 ceramics shows the higher d_{33} value than those $BaTiO_3$–Air ceramics. The related mechanism will be discussed later. Below that, it is just reverse. The lower relative density may be responsible for that, as shown in Table 1. Generally, it is considered that the sintering atmosphere has greatly influence on the g dependence of piezoelectric properties.

It is known that the piezoelectric properties of a piezoelectric ceramics material could be generally resolved into intrinsic and extrinsic contributions. The former originates from the deformation of the unit cell under an external electric or mechanical field, while the latter is mainly due to domain wall movement [5, 6, 12–15]. Obviously, both the piezoelectric grain-size effects are closely related to the extrinsic contributions.

Figure 4 presents SEM images of domain structure observed in the poled $BaTiO_3$–Air and $BaTiO_3$–O_2 with different sintering temperature. The evolution of the microstructure and domain structure can be clearly seen from these figures. As shown, below 1210 °C, most of the grains are of single domain structure. This may be another reason for the great decrease of d_{33} values below 1210 °C for $BaTiO_3$–Air and $BaTiO_3$–O_2 atmosphere. The extrinsic contribution to d_{33} from the domain wall motion will reduce as the amount of domain walls decrease. Above 1210 °C, stripes and herringbone patterns are recognizable inside the grains. These have been reported to be typical features of the domain configuration of $BaTiO_3$ ceramics in the tetragonal phase [6, 16, 20–23]. The stripes correspond to the 90° domain patterns, where polarization vectors in adjacent domains adopt a head-to-tail arrangement across the domain boundaries. The physical origin of the formation of 90° domains is considered to be associated with the release of internal stress. The herringbone patterns are the consequence of the combination of two sets of alternating 90° domains [6, 10–12, 20]. Furthermore, it can be found that the domain configuration become more complex with the increase of the g in both groups of the $BaTiO_3$ ceramics. The domain patterns of the fine-grained $BaTiO_3$ ceramics are quite simple, being predominantly stripes. While, for coarse-grained $BaTiO_3$ ceramics, diverse and very complicated domain patterns are more frequently observed. However, the critical g for the appearance of the herringbone domain patterns is different. For the $BaTiO_3$–Air ceramics, with the fine grain ($g \approx 1$ μm), the domain patterns mainly consist of stripes patterns running across the whole grain, as shown in Fig. 4c. Small amount of herringbone domain patterns could be found with g larger than 2 μm, shown in Fig. 4e. With increase the g, more and more herringbone domain patterns are frequently observed. However, for the $BaTiO_3$–O_2 ceramics, nearly no herringbone domain patterns could be observed inside the grain until the g is larger than 7.3 μm.

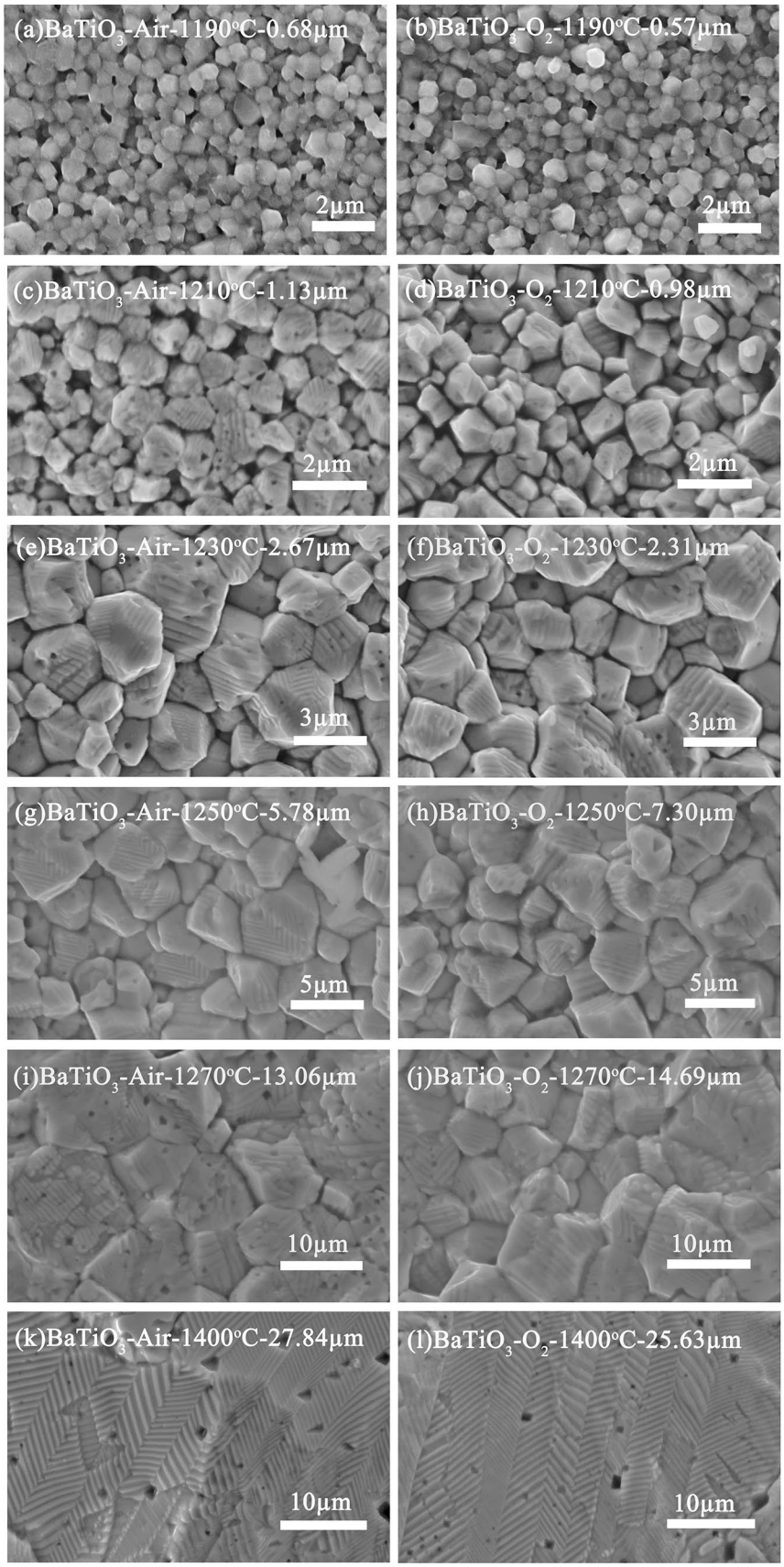

Fig. 4 Domain structures of poled $BaTiO_3$ ceramics under different sintering atmospheres with different sintering temperature

Domain width (w) is considered to be an important reason for the piezoelectric grain-size effects of $BaTiO_3$ ceramics [4, 6, 17–19]. Small w leads to high domain density are considered to account for the strong piezoelectric activities in the fine-grain $BaTiO_3$ ceramics [9–13, 23]. Figure 5 illustrates the change in the average w with g for the various poled $BaTiO_3$ ceramics of sintering under different atmospheres. The domain width was calculated by linear intercept method. Each line was vertical through a series of parallel domain. Then the total length of the lines was measured using the scale and the total grain number was counted. The domain width was statistically averaged in more than 150 grains at different locations for each specimen [5, 8, 9, 25–29]. As shown, the average w decreases with decreasing g for both groups of $BaTiO_3$ ceramics. At the same g, the $BaTiO_3$–O_2 ceramics exhibits smaller w than the $BaTiO_3$–Air ceramics. It may be the reason for the larger d_{33} values of the $BaTiO_3$–O_2 ceramics compared with that of the $BaTiO_3$–Air ceramics with the larger g above 2 μm. However, the similar g dependence of w obviously cannot account for the different piezoelectric grain-size effects mentioned above. This phenomenon demonstrates that the w is not the only reason for the piezoelectric grain-size effects. Systematic studies of the domain structures are needed.

Interestingly, it seems like that the different piezoelectric grain-size effects under different sintering atmospheres are closely related to the critical g variations of appearance of herringbone domain patterns. For the $BaTiO_3$–Air samples, herringbone domain patterns gradually increase with the increase of g over 1 μm. At the same time, the d_{33} gradually decreases with the increase of g and exhibits a sharp peak at g near 1 μm. While for the $BaTiO_3$–O_2 samples, nearly no herringbone domain patterns could be observed inside the grain until the g is larger than 7.30 μm. Simultaneously,

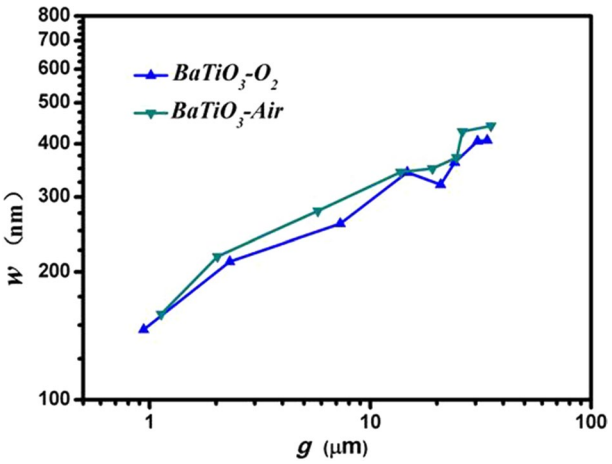

Fig. 5 Grain-size dependences of domain width of $BaTiO_3$ ceramics under different sintering atmospheres

the d_{33} value begins to decrease with the increasing g. It has been revealed that the herringbone domain patterns have greatly influences on the piezoelectric grain-size effects of $BaTiO_3$ ceramics. The motion of a 90° domain wall might be inhibited by the interactions from the neighboring domain walls that are included in the complex and conjoined herringbone domain patterns [28–33]. In such a case, it might be more proper to consider the motion of domain walls as the joint behavior, which will increase the effective inertia mass for an individual domain wall [9, 23–27]. This will reduce the domain walls' response to the external electrical or stress signal, reduce the extrinsic contribution of domain wall motion to piezoelectric activities and lead to the lower d_{33} value [6, 9, 16–25]. Therefore, the herringbone domain patterns are considered to be the more important factor that decreases the piezoelectric activities in the coarse grains [13, 20]. The experiment results above indicate that the herringbone domain patterns may be also accountable for the decrease of piezoelectric activities in the fine grains.

Furthermore, the mentioned above experiment results also demonstrate the formations of the herringbone domain is closely related to the oxygen defects in the grain [26–32]. It can be easily understand as the oxygen defects will introduce large internal stress in the grain [14, 31–39]. Herringbone domains patterns forms as the stress could not be relieved by the 2-dimensions adjustment. In the fine-grained ceramics, oxygen defects inner the grain can be easily compensated in the oxygen sintering atmosphere due to the small g and low sintering temperature [32–35]. Therefore, the herringbone domain patterns are greatly decreased [26, 27]. But in the coarse-grained $BaTiO_3$ ceramics, the compensation of inner oxygen defects is difficult because of the large g and high sintering temperature [35–38]. Correspondingly, the oxygen cannot inhibit the formation of herringbone domain patterns any more.

4 Conclusions

The influences of sintering atmosphere on piezoelectric grain-size effects were systematically studied in this paper. It is indicated that the appearance of herringbone domain patterns should be responsible for the decreases of the piezoelectric activities in both coarse grains and fine grains. Oxygen atmosphere can delay the formation of the herringbone domain by reducing the oxygen defects, which will decrease the inner stress of the samples. The variations of critical g for appearance of the herringbone domain patterns might be an important reason for the different piezoelectric grain-size effects under different sintering atmospheres.

Acknowledgements This work was supported by the National Natural Science Foundation of China [Grant No. 51302056, 51502067 and 51302124] and the Natural Science Foundations of Zhejiang Province [Grant No. LQ16E070002].

References

1. B. Jaffe, W.R. Cook, H. Jaffe, *Piezoelectric Ceramics*. (Academic Press, London, 1971)
2. Y. Saito, H. Takato, T. Tani, T. Nonoyama, K. Takatori, T. Homma, T. Nagaya, M. Nakamura, Adv. Mater. **125**, 130–170 (2010)
3. L.E. Cross, Nature **432**, 24–25 (2004)
4. T. Hoshina, K. Takizawa, J. Li, T. Kasama, H. Kakemoto, T. Tsurumi, Jpn. J. Appl. Phys. **47**, 7607–7611 (2008)
5. L. Zheng, S. Li, S. Sang, J. Wang, X. Huo, R. Wang, Appl. Phys. Lett. **105**, 212902–212906 (2014)
6. T.R. Shrout, S.J. Zhang, J. Electroceram. **19**, 251–257 (2007)
7. P. Zheng, J.L. Zhang, Y.Q. Tan, C.L. Wang, Acta Mater. **60**, 5022–5030 (2012)
8. S. Wada, K. Yako, H. Kakemoto, T. Tsurumi, T. Kiguchi, J. Appl. Phys. **98**, 014109-014109-7 (2005)
9. H.T. Martirena, J.C. Burfoot, J. Phys. C Solid State Phys. **7**, 3182–3192 (2001)
10. S.M. Moon, X. Wang, N.-H. Cho, J. Ceram. Soc. Jpn. **117**, 729–731 (2009)
11. M. Eriksson, H. Yan, G. Viola, H. Ning, D. Gruner, M. Nygren, J. Am. Ceram. Soc. **94**, 3391–3396 (2011)
12. S. Wada, K. Takeda, T. Tsurumi, T. Kimura, Jpn. J. Appl. Phys. **46**, 372–376 (2007)
13. Y. Tan, J. Zhang, Y. Wu, C. Wang, V. Koval, B. Shi, Sci. Rep. **5**, 9953 (2015)
14. J.L. Zhnag, P.F. Ji, Y.Q. Wu, X. Zhao, Y.Q. Tan, C.L. Wang, Appl. Phys. Lett. **104**, 222909-222909-4 (2014)
15. K. Kinoshita, A. Yamaji, J. Appl. Phys. **47**, 371–373 (1976)
16. H. Takahashi, Y. Numamoto, J. Tani, K. Matsuta, J. Qiu, S. Tsurekawa, Jpn. J. Appl. Phys. **45**, L30–L32 (2006)
17. T. Karaki, K. Yan, M. Adachi, Jpn. J. Appl. Phys. **46**, 7035–7038 (2007)
18. P. Zheng, J.L. Zhang, S.F. Shao, Y.Q. Tan, C.L. Wang, Appl. Phys. Lett. **94**, 032902–092902-3 (2009)
19. H. Yu, X. Wang, F. Jian, L. Li, J. Am. Ceram. Soc. **96**, 3369–3371 (2013)
20. J.F. Chou, M.H. Lin, H.Y. Lu, Acta Mater. **48**, 3569–3579 (2000)
21. N. Ma, B.P. Zhang, W.G. Yang, D. Guo, J. Eur. Ceram. Soc. **32**, 1059–1066 (2012)
22. D. Damjanovic, J. Appl. Phys. **82**, 1788–1797 (1997)
23. J.C. Wang, P. Zheng, R.Q. Yin, L.M. Zheng, J. Du, L. Zheng, Ceram. Int. **41**, 14165–14171 (2015)
24. S. Li, W. Cao, L.E. Cross, J. Appl. Phys. **69**, 7219–7224 (1991)
25. W. Cao, Nat. Mater. **4**, 727–728 (2005)
26. T. Matsui, M. Kondo, A. Matsuda, Jpn. J. Appl. Phys. **42**, L901–L903 (2003)
27. P. Baxter, N.J. Hellicar, B. Lewis, J. Am. Ceram. Soc. **38**, 412–418 (1955)
28. F. Yu, W.L. Li, X. Dan, Y.L. Qiao, Z. Y. Yang Yu,: Acs. Appl. Mater. Inter. (2016)
29. I.A. Yunaz, A. Yamada, M. Konagai,Jpn. J. Appl. Phys. **46**, L1152–L1154 (2007)
30. T. Oyama, N. Wada, H. Takagi, M. Yoshiya, Phys. Rev. B **82**, 1456–1461 (2010)
31. Y.K. Choi, T. Hoshina, H. Takeda, T. Tsurumi, Jpn. J. Appl. Phys. **50**, 031504-031504-5 (2011)
32. R. Hemphill, L. Bellaiche, A. Garcı´a, D, Vanderbilt, Appl. Phys. Lett. **75**, 4111 (2006)
33. A.K. Tagantsev, I. Stolichnov, E.L. Colla, N, Setter. J. Appl. Phys. **90**, 1387–1402 (2001)
34. L. He, D. Vanderbilt, Phys. Rev. B **68**, 399–404 (2003)
35. R. Waser, J. Am. Ceram. Soc. **71**, 58–63 (1988)
36. G. Arlt, P. Sasko, J. Appl. Phys. **51**, 4956–4960 (1980)
37. Q.M. Zhang, H. Wang, N. Kim, L.E. Cross, J. Appl. Phys. **75**, 454–459 (1994)
38. M. Dawber, J.F. Scott, Appl. Phys. Lett. **76**, 1060–1062 (2000)
39. R. Ahluwalia, W. Cao J. Appl. Phys. **89**, 8105–8109 (2001)